

Energy Sensitive Imaging of Focused and Scanning Ion Microbeams with μm Spatial and μs Time Resolution

Carlos Granja^{1*}, Cristina Oancea¹, Anna Mackova^{2,3}, Vladimir Havranek², and Vaclav Olsansky^{2,4}

¹Advacam, U Pergamenky 12, 170 00 Prague 7, Czech Republic

²Nuclear Physics Institute, Czech Academy of Sciences, Husinec 130, 250 68 Rez, Czech Republic

³Faculty of Science, J. E. Purkinje University, Pasteurova 1, 400 96 Usti nad Labem, Czech Republic

⁴Faculty of Mechanical Engineering, Czech Technical University in Prague, Technicka 4, 160 00 Prague 6, Czech Republic

Abstract. We inspected and imaged the delivery of ion microbeams with spatial, time and energy sensitivity. Quantum imaging registration event-by-event is provided in high spatial and time resolution with the position-sensitive semiconductor pixel detector Timepix. The detector is operated as a miniaturized radiation camera for flexible measurements at room temperature and in vacuum. Imaging information on beam profile, spatial and time distribution, flux, homogeneity, and deposited energy for individual beam particles is provided. Focused and scanning beams can be imaged and evaluated online. Single particles are registered by the detector including spectral (deposited energy) information on their position at the μm and μs level. Delivered beams can be characterized also in terms of composition by resolving background and unwanted components such as electrons and X rays from primary beam particles. Ion groups of different energy including doublets or scattered particles can be identified. The technique is applicable for ions of energy above few hundred keV and beams of low intensity, below 10^5 particles/cm²/s.

1 Introduction and motivation

Particle accelerators with advanced beam delivery systems provide highly precise, spatially tailored and time-stamped scanning beams at the micrometer scale [1]. It is desirable to independently verify and monitor with sufficient resolution the delivery of such microbeams. The characterization and spatial mapping of such microbeams would ideally include parameters such as beam size, spatial and time distribution, particle composition, direction and deposited energy. Such requirements and related applications can be found in ion beam analysis (IBA) studies, such as scanning ion transmission microscopy (STIM) [2] and ion beam lithography [3].

* Corresponding author: carlos.granja@advacam.com

These tasks can be addressed by high-granularity imaging detectors such as the hybrid semiconductor pixel detector Timepix [4] which provides spectral and tracking response at the pixel level with high resolution for a wide range of particle types [5-7]. Extensive information and high spatial resolution are achieved by placing the pixel in the particle beam (for low beam intensities) and registering single-particle tracks. Detailed event-by-event processing enables particle identification and spectral tracking response to single particles [7-8]. Such high-resolution mode can be applied on a wide variety of radiation fields with particle flux up to about 10^5 particles/cm²/s (equivalently, up to 10^{-1} pA beam current intensity). The limit of beam flux at which the detector operates in high-resolution event-by-event detection, is set by the particle type, the particle direction and energy loss in the detector sensor [5]. The Timepix detector operates in frame mode with exposure time for example at the \approx ms level or preferably longer. This level ensures the detector proper operation and complete collection of the deposited charge especially by high energy loss particles especially ions.

The detector and developed technique can be also applied to the evaluation, imaging and monitoring of ion beams of larger beam size at the mm and cm scale [9-10]. Existing ion-beam monitoring sensors such as single-pad detectors have limited resolving power and narrow field-of-view (FoV) requiring the use of collimators. Track-etch detectors provide high spatial resolution but require offline processing. On the other hand, high-sensitivity pixel detectors with integrated electronics provide online response, high spatial resolution, wide FoV, spectral-tracking response and enhanced sensitivity for precise measurements [11]. The pixel detector implemented in miniaturized readout electronics stands as a compact highly integrated camera [6] which can be mounted without complexity and operated by standard computer.

2 Instrumentation and measurements

2.1 Miniaturized radiation camera MiniPIX TPX

Position-sensitive detection of single particles with energy and time information can be provided with high-resolution by the hybrid semiconductor pixel detector Timepix [4]. The detector consists of the Timepix ASIC chip bump bonded to a semiconductor radiation-sensitive sensor. The Timepix detector operates at room temperature including also measurements in vacuum. The detector was equipped with a 300 μ m thick silicon sensor which was operated with a relatively low applied bias (+30 V) in order to suppress the per-pixel high-energy saturation and enhance the charge sharing effect. Timepix provides a high granularity matrix of independent pixels of total sensitive area 1.98 cm² (256 rows \times 256 columns = 65.536 pixels of total size of sensitive area 14 mm \times 14 mm = 1.98 cm²) – see Figure 1a.

Timepix registers single particles and measures at the pixel level the deposited energy, event count rate or time of interaction. The detector is operated with integrated power and readout electronics provided by the miniaturized radiation camera MiniPix TPX [6] shown in Figure 1b. The device is controlled and readout by single USB 2.0 cable to a standard PC or laptop running the cross-platform software tool PIXET.

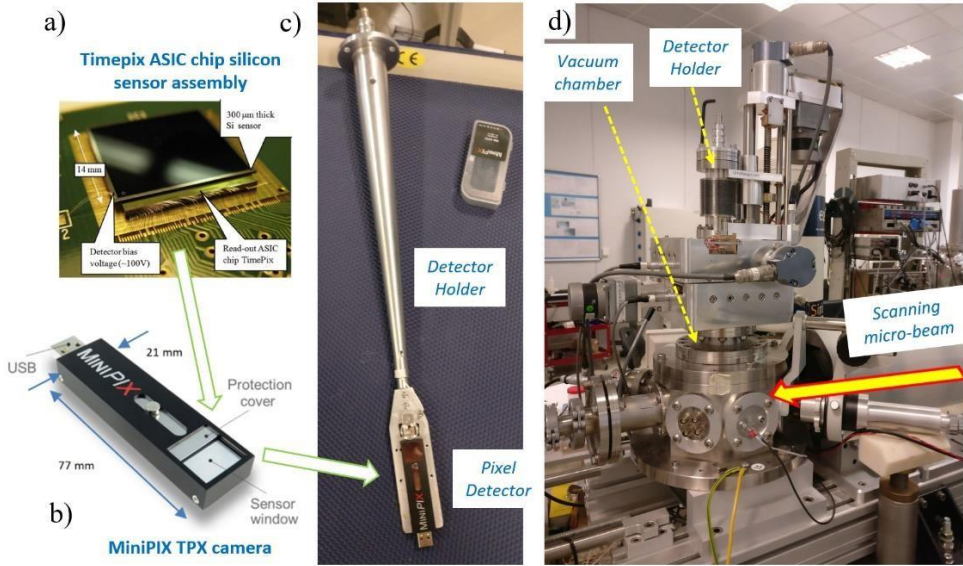


Fig. 1. (a): Pixel detector Timepix ASIC chip – silicon sensor (300 μm thick silicon) assembly. (b) Miniaturized radiation camera MiniPIX TPX operated at room temperature and in vacuum. (c) Detector and holder with thermal contact for passive cooling. (d) Experimental vacuum chamber at the microbeam guide at the Tandatron 4130 MC accelerator, NPI CAS in Rez.

2.2 Ion microbeams at the NPI Tandatron

In this work we used microbeams of ^{12}C ions of two energies (4 MeV and 10 MeV) delivered by the 4130 MC Tandatron accelerator of the NPI CAS Rez [1]. Measurements were performed in vacuum ($< 10^{-5}$ mbar) at the microbeam guide. Focused and scanning microbeams delivered in various modes and configurations in terms of energy, spatial and time distribution were examined and evaluated.

2.3 Measurements

The spatial scanning mode of beam delivery was studied. Adjustable accelerator beam parameters tested included: beam spot size, irradiated beam area, spatial scanning modes and frequencies, beam profile, flux and time distribution. The Timepix detector was operated and readout in frame mode. Depending on the beam flux and event rate at the detector position the frame acquisition time was set in the range from hundreds of μs to few seconds in order to register isolated particle tracks and keep the pixel occupancy low ($< 10\%$). The detector pixels operation mode was used on different measurements on time-over-threshold (ToT) energy mode, designed for precise energy loss registration, or time-of-arrival (ToA) mode, designed for detailed time registration. The detector was operated and readout by standard PC/notebook running Windows using the PIXET software. Raw data were processed offline.

3 Methods and results

3.1 Correlated detection: position, time, deposited energy

The Timepix detector registers single particles in the form of pixelated tracks, called *clusters*, as shown in Figure 2. The charge deposited by charged particles in the center of the cluster is spread out into neighboring pixels due to charge sharing in the semiconductor sensor at room temperature [5,12]. This effect enables to determine, by model fitting of the pixelated cluster, the position of interaction with sub-pixel resolution. For heavy charged particles, such as ^{12}C ions, the spatial resolution can reach the μm level [12]. At the frame level Timepix measures in high resolution for each particle the position and the deposited energy or the position and the time of interaction as shown on top and bottom rows of Figure 2, respectively.

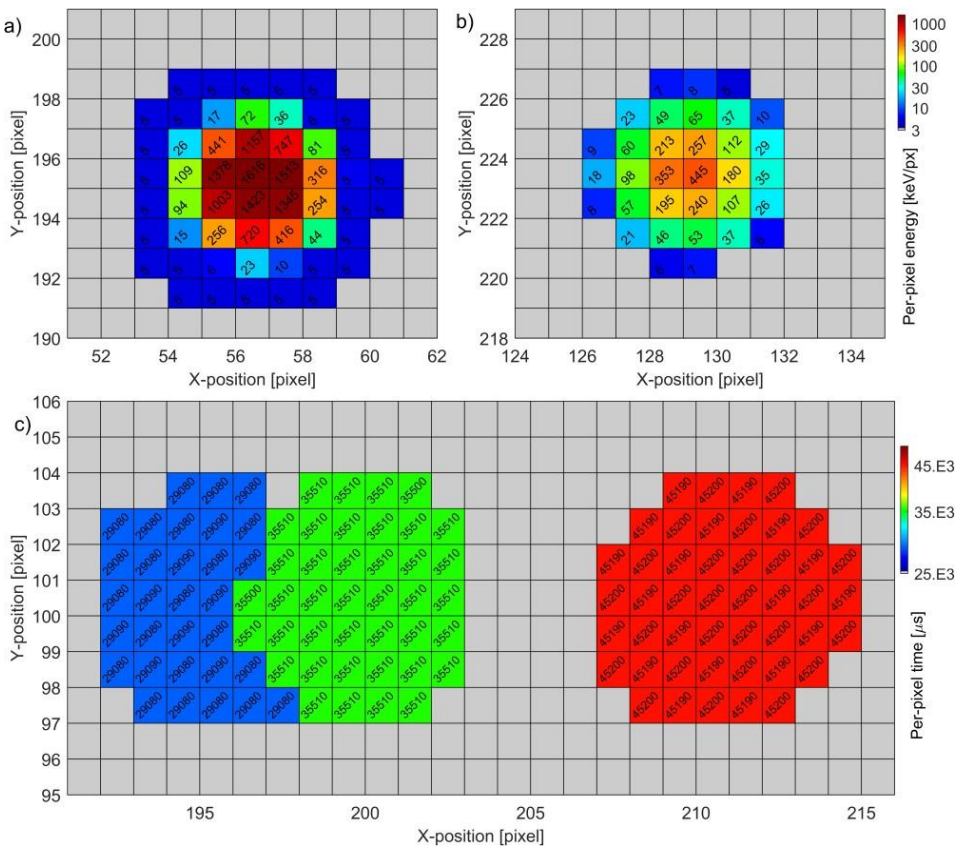


Fig. 2. Spectral- and time-sensitive imaging detection of single ions by the pixel detector Timepix with a $300\ \mu\text{m}$ silicon sensor operated in per-pixel *energy* (top row) and *time* (bottom row) modes. Pixelated tracks, called clusters, are shown for single ^{12}C ions of energy 10 MeV (a) and (c) and 4 MeV (b). The per-pixel energy in keV or time in μs are displayed by the color bar (exact values are typed in the hit-pixels). A small portion of the Timepix detector area is shown – on the top row: 11×11 pixels = $605\ \mu\text{m} \times 605\ \mu\text{m} = 0.37\ \text{mm}^2$, and on the bottom row: 11×25 pixels = $605\ \mu\text{m} \times 1375\ \mu\text{m} = 0.83\ \text{mm}^2$.

Information on the deposited energy can be recorded in high energy resolution operating the detector in per-pixel (called time-over-threshold ToT) energy mode – see Figure 2, top row, displayed in keV per pixel. The particle deposited energy is given by the sum of the per-pixel energies (shown in color) over the hit pixels in the cluster.

Information on the time of interaction at the pixel level can be measured by operating the detector in time-of-arrival (ToA) mode as shown in Figure 2c. The time-of-interaction registered at the per-pixel level with μs level resolution is displayed by the color bar in Figure 2c. The range and time resolution can be adjusted by varying the value of the Timepix high-frequency clock. Typical values are listed in the Table 1. The extent is given by the per-pixel readout range of 11.810 bins [4]. Each particle registered in the detector is thus assigned a time stamp with resolution at the μs level.

Table 1. Time range and resolution for time-of-arrival (ToA) operation of Timepix. Values are given for selected values of the detector high-frequency clock commonly used.

Timepix clock	Time range	Time resolution
10 MHz	1.8 ms	0.1 μs
1 MHz	11.8 ms	1 μs
100 kHz	118 ms	10 μs
10 kHz	1.18 s	100 μs

Two or more particles can interact in the same spatial region of the detector during the same frame acquisition interval. The resulting overlapping signal in the detector, see doublet event in Figure 2c on left, can be resolved when Timepix is operated in time mode. This setting can be used to examine highly focused and spatially scanning microbeams.

Operating the detector in time mode it is still possible to derive limited information on the particle deposited energy. This is possible by exploiting the spectral sensitivity of the size of the pixelated clusters (i.e., the number of pixels in the cluster). This can be observed in Figure 2 between the registration of ^{12}C ions of 10 MeV and 4 MeV, respectively. By taking into account also the morphology-tracking response of Timepix it can be also derived information on particle-event type [5]. This is possible by cluster morphology and pattern recognition analysis of the characteristic pixelated tracks of Timepix to radiation components in terms of particle types, such as X rays, electrons, protons and ions [5].

3.2 Time-correlated spatial mapping of ion microbeam spot

The time-stamped spatial distribution of single particles from a scanning microbeam of 10 MeV ^{12}C ions is shown in Figure 3. The microbeam was set to a scanning region of spot area of $1\text{mm} \times 1\text{mm}$ and scanning speed of $4 \mu\text{m}/\text{ms}$. The beam covered the entire spot region once in nearly 5 min 30 sec during which around 700 particles were registered by the detector in over 11 k Timepix frames of 10 ms acquisition time. The detector live time (113 s) is about one third (34.5 %) of the total beam spot time irradiation (327 s). The detector deadtime of each frame readout was 19 ms. Due to the detector deadtime of frame readout, the detected particles are just about one third of all particles delivered by the microbeam. Particles are also detected beyond the scanning beam region as can be seen in the image map. The incidence and time and spatial characteristics of such events can be evaluated (subject of future work).

The Timepix detector was operated in time mode (see Figure 2c and Figure 3) for registration of single particles with high timing resolution. For the particles used, light ions, the position of interaction, called centroid of the cluster, in the detector is determined with sub-pixel spatial resolution at the few μm level. The resulting spatial image is produced as the map of the centroid of interaction of the single particles which can be displayed with

spatial bin of size above this level. Given the low event rate by the microbeam flux, and limited detector live time, the spatial bin size in the image shown in Figure 3 was set to size $10\ \mu\text{m}$. The entire spatial cluster, which involves many of the detector pixels and extends to several hundreds of μm (see Figure 2), is not displayed in the imaging map of the microbeam scanning spot region.

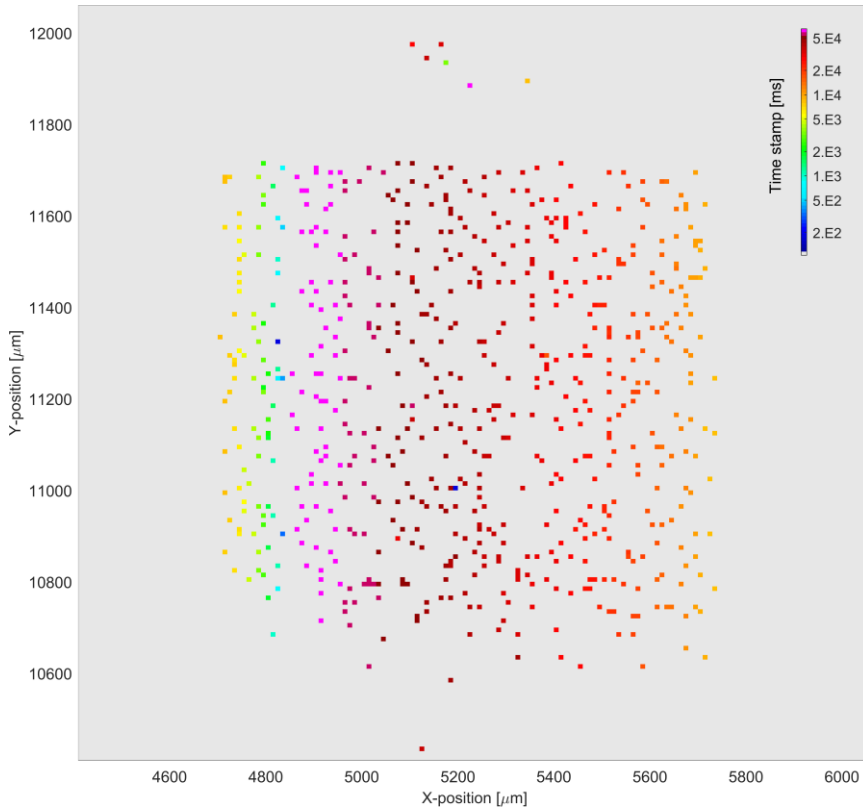


Fig. 3. Time-sensitive spatial distribution of single $10\ \text{MeV}\ ^{12}\text{C}$ ions in a scanning microbeam of area $1\ \text{mm} \times 1\ \text{mm}$, scanning speed $4\ \mu\text{m}/\text{ms}$. Data shown for one full scan over the scanning spot area irradiated in $327\ \text{s}$ (of which $113\ \text{s}$ was the total live time of the detector). The time-of-detection of the single ions in the detector is shown in color in ms. Only the particle hit centroid position is displayed in the plot spatial binning size of $10\ \mu\text{m}$. Data registered by the MiniPIX Timepix detector operated in per-pixel time-of-arrival mode. Only a part of the detector pixel matrix area ($1.4\ \%$) is shown (30×30 pixels = $1.65\ \text{mm} \times 1.65\ \text{mm} = 2.72\ \text{mm}^2$).

3.3 Spectral-correlated time histogram of delivered ion position

The detailed time distribution of the single particles registered by the detector can be evaluated. The time histograms of the position of the detected ions along the X and Y axis of the detector are shown in Figure 4. The same data of Figure 3 is used. The time range is partly extended (from $65\ \text{s}$ to $80\ \text{s}$) which contains one entire spatial scanning over the microbeam spot area with additional $15\ \text{s}$ of the next beam scan in order to show the spatial scanning pattern along the X and Y axis directions.

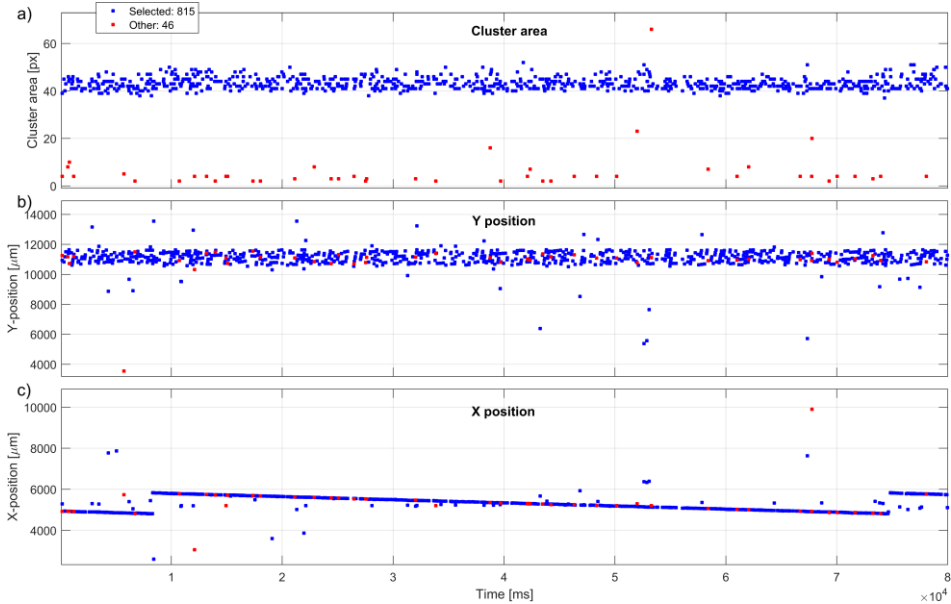


Fig. 4. Time histograms of detection of single ions by Timepix. The plots show the values of (a) cluster size, (b) Y position and (c) X position for the single particles. Results shown for the same data of Figure 3. Two groups of particles are resolved: primary beam particles – 10 MeV ^{12}C ions – blue (815) and other particles – red (46). The evaluated time interval, plotted on the horizontal axis, is extended to 80 s (from 65 s – interval of one complete spatial spot scan by the beam). See text.

Figure 4 includes the cluster size (number of pixels) of the registered particles in the detector. This quantity is proportional to the deposited energy. ^{12}C ions of 10 MeV and 4 MeV produce clusters of different area: of around 50 and 30 pixels, respectively – see Figure 2. Together with additional cluster morphology parameters such as cluster linearity and roundness, these quantities can be used to resolve particle-event types and thus characterize the composition of the radiation field [5]. Primary beam ions can be discriminated from background and unwanted events such as electrons, X rays, scattered particles and ions of different energy.

The correlated spatial- and time-information can be used to examine and characterize the deposited beam in terms of the composition (particle types) of the delivered beam, time and position of delivery with μs and μm level resolution, respectively.

3.4 Time-sensitive distance travelled of ion microbeam spot

The spatial trajectory of the microbeam spot delivery can be inspected and evaluated by Timepix at the μm spatial and μs time resolution level. We evaluated the beam *travelled distance*, expressed as the consecutive distance between delivered single ions on the detector sensor plane. The value of this quantity along the irradiated time is shown in Figure 5. Results are presented for the same data of Figure 3 (and of Figure 4 in the 65 s interval of an entire scan over the spot region). The travelled distance can be expressed in 2D (shown in black) or along the X- and Y- axis components (shown in blue and red, respectively).

The results shown, in Figure 5, Figure 4 and Figure 3, are produced by the particles detected in the detector. Thus, due to the detector readout dead time, they represent about one third of all irradiated particles by the beam during the same time interval evaluated.

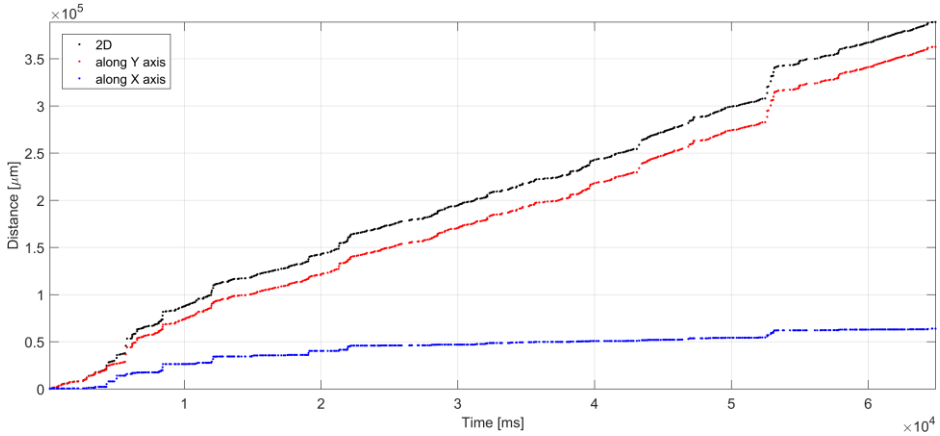


Fig. 5. Traveled distance of the 10 MeV ^{12}C microbeam for the data in Figure 3. The quantity (data points in black) can be also evaluated along the detector axis Y direction (red) and X direction (blue).

3.5 Ion microbeam imaging: particle rate map

We investigated the delivery and spatial visualization of a 4 MeV ^{12}C ion scanning microbeam of customized spatial pattern of scanning area $600\ \mu\text{m} \times 700\ \mu\text{m}$ and scanning step of $3.9\ \mu\text{m}$ (resulting from the beam spot binning $1\ \text{mm} / 256$ steps) – see Figure 6. The customized beam pattern was in the form of a pre-defined image produced by the Tandetron scanning microbeam system which was defined over a bit map such as those used in ion beam lithography.

Figure 6 shows the integrated particle count per image spatial bin registered by the detector. As in Figure 3, the image spatial bin size was also set to $10\ \mu\text{m}$. The data shown were collected in 5 min during which the beam performed several scans over the scanned area. A total of 3012 ions were registered by the detector during this interval. Over 10 k Timepix frames of acquisition time 10 ms were collected. The total detector frame exposure time (103 s) gives a total live time of 35%. Thus, the actual number of ions delivered is about twice as many as those registered. The number of non-empty spatial image bins, i.e., containing one or more events, in the entire imaged region displayed is 1827.

In this measurement the Timepix detector was operated in ToT per-pixel energy mode and readout in frame mode with acquisition time 10 ms. The detector frame acquisition time was set at this level in order to register single particles and avoid event pileup while maximizing detector exposure live time.

In a given Timepix frame, with the detector per-pixel operation set in energy mode, particles arriving at different detector regions are separated and can be distinguished. However, when the particles arrive to the same detector position in the given frame *event pileup* in the detector can occur. This means two or more particles appear registered as one particle of higher deposited energy in the detector giving rise to *event energy multiplets*. This effect in the detector can account for high-energy groups in the deposited energy spectrum (see Sec. 3.6).

The number of delivered ions (Figure 6) gives the event rate and total fluence in the evaluated region and scanned time interval. The beam spatial deposition and homogeneity are visualized and can be evaluated. It can be observed a distribution of values in the pattern image ranging from 0 (no events) up to six events per spatial bin. The beam composition in terms of main particle-type groups can be derived by the detector resolving power and pattern recognition analysis of the pixelated tracks [7]. In the results presented,

all detected particles are processed and shown. The radiation field at the detector position was quite pure, containing primarily the microbeam particles, i.e., ^{12}C ions. If necessary, background and unwanted particles, such as electrons and X rays, can be filtered out by the detector particle-type resolving power and spectral-tracking sensitivity [7].

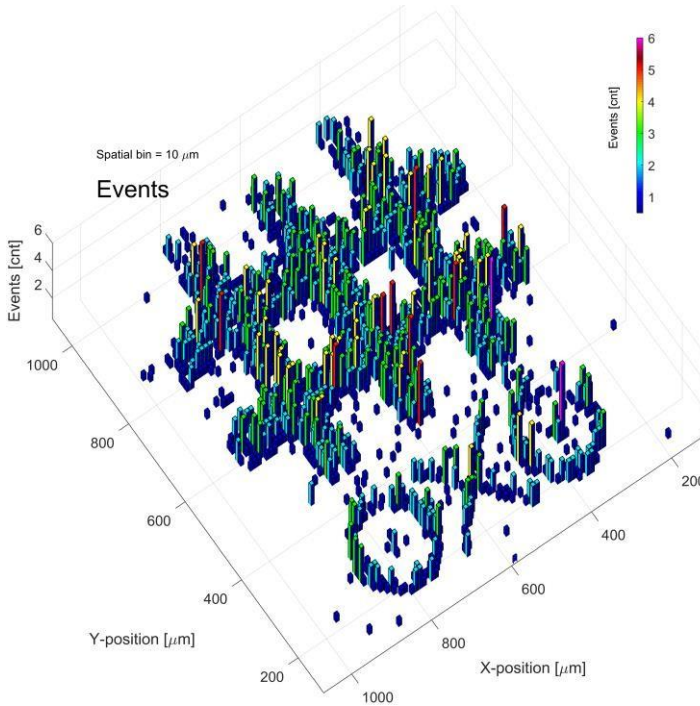


Fig. 6. Spatial distribution of ion delivery of a 4 MeV ^{12}C scanning microbeam with customized spatial pattern of size $600\ \mu\text{m} \times 700\ \mu\text{m}$ registered by Timepix. Total beam irradiation time 5 min, during which time the beam scanned the spot region several times. The number of events (**event rate** – evaluated per image spatial bin, set of size $10\ \mu\text{m}$) is displayed in the vertical axis and in the color bar scale. A small portion of the pixel detector area (0.74%) is shown (22×22 detector pixels = $1.21\ \text{mm} \times 1.21\ \text{mm} = 1.46\ \text{mm}^2$).

3.6 Ion microbeam imaging: deposited energy map

The spatial distribution of deposited energy by single particles can be evaluated also at the μm scale. The same data set used in Figure 6 is processed and displayed in terms of deposited energy according to the same spatial image binning as given in Figure 7. When two and more events were registered in different detector frames and correspond to the same spatial bin, the average value is displayed in the spatial image. Similar to the event rate image above, a range of values is observed over the scanned spot region. In terms of deposited energy several group values are registered by the detector in the range from 2 MeV to nearly 14 MeV. Most events in the detector were registered with the lowest energy group (see discussion below). In the evaluated data set, containing several scanning sweeps by the beam, most spatial bins in the pattern correspond to the lowest energy peak. The other higher energy multiplet groups are observed in decreasing incidence. There are also bins without any values which correspond to image spatial bins without any events – see discussion in Sec. 3.5.

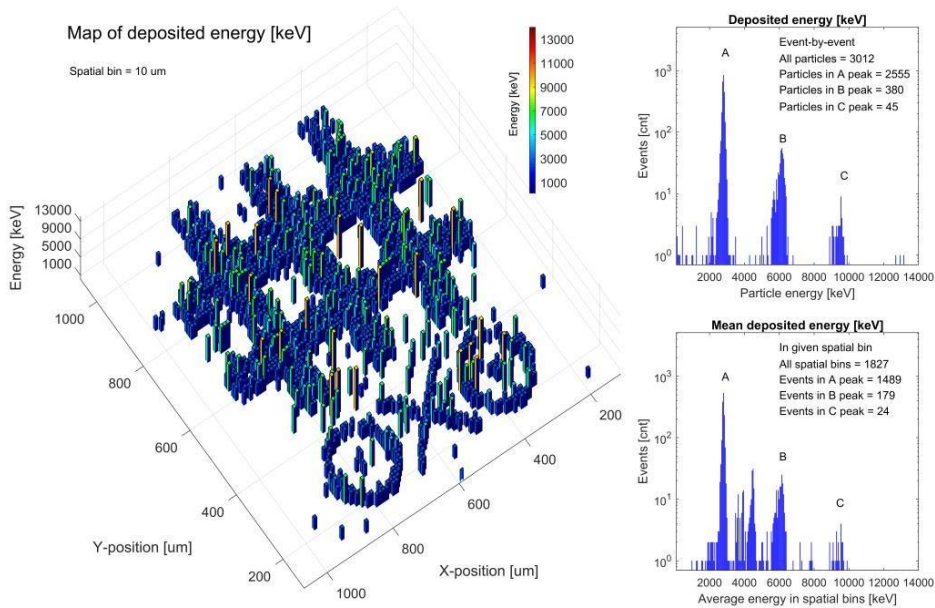


Fig. 7. Same as Figure 6 showing the ion **deposited energy** per spatial bin (displayed in the vertical axis and in color). For spatial bins registering two and more ions, the average value of ion deposited energy is displayed. The deposited energy spectrum of single ions is included (top right). The resulting distribution of averaged energies evaluated according to the spatial bins of the image is also shown (bottom right). See text.

3.7 Ion microbeam spectrometry: deposited energy spectrum

In addition to the spatial distribution of single particle delivery, the deposited energy spectrum can be measured and evaluated. The resulting distribution for the event-by-event processing is given in Figure 7 (top right). The spectrum measured by the detector shows a dominant low-energy component with peak centroid at around 2.8 MeV. This component corresponds to the primary beam mono-energetic particles. The difference in energy from the accelerator value (4 MeV ^{12}C ions) can result from non-negligible energy loss in the detector thin insensitive electrode layer ($\approx 1 \mu\text{m}$, Aluminum) significant for heavy charged particles and the limited energy resolution of the detector especially in the high energy region. The detector per-pixel calibration is performed with X rays and gamma rays in the low energy region [12]. The detector energy resolution, for high-energy loss particles such as ions, is at the level of 8% [5,14]. Another source of loss of charge collected is the incomplete sensor depleted volume (estimated at around 60%), due to the insufficient applied bias. The low bias was chosen in order to suppress the per-pixel high-energy distortion and enhance the charge sharing effect.

In the event-by-event spectrum Timepix registers additional higher-energy groups. Their positions appear at multiple values of the first low-energy group. This points out to occurrence in the detector of multiplet events making three groups: doublets, triplet and a four-fold component of energies at around 6, 9.7 and 13 MeV, respectively. These higher-order groups registered by the detector appear as single particles of multiple-fold energy. They can however be two and more single particles arriving to the pixel detector within the

detector acquisition time (10 ms) and in the same spatial position at the detector pixel size level, i.e., 55 μm . Such events cannot be resolved by Timepix operated in per-pixel energy mode. They could be resolved by operating the detector in counting mode, for which however the energy sensitivity of Timepix becomes limited.

Taking into account the imaging information, the spatially-correlated spectrum of deposited energy can be evaluated. In the case when more events are registered in the same image spatial bin (in the results shown the spatial bin is set to 10 μm), the averaged deposited energy per spatial bin is shown as the spectral image – Figure 7 (left) and as the energy spectrum – see Figure 7 (bottom right).

Due to the detector limited exposure live time, many of the delivered particles (about twice as many) are not registered. This effect in the detector can partly account for the inhomogeneity of ion registration over the scanned spatial pattern. Similarly, the total number of non-empty spatial bins for the data and interval processed (1827) is therefore smaller than the total number of particles registered by the detector (3012). The event occupancy values according to the large component groups, revealed in the event-by-event spectrum (Figure 7 top right), are included in the plot – see text inset in Figure 7. It can be noted an additional component appears between the first and second component of the event-by-event results. This results from the averaging of two and more events in a given spatial bin, which were registered with different energy values in the event-by-event data.

The deposited energy distributions results, processed as event-by-event particles or as spatially binned events (Figure 7) can be used to derive information on event rate, particle energy loss and deposited dose in the scanned spot region. Application of this technique is used in energy-sensitive particle radiography [13] in which few particles, even just one, are needed in each image bin to produce imaging contrast of thin samples. The correlated time information is also registered and can be evaluated for homogeneity of beam spot delivery.

The combined results provide a detailed and complete mapping of the delivered beam. Spatial and time distribution are measured in terms of number of particles, deposited energy, energy loss and time. For heavy charged particles the images can be produced with sub-pixel spatial resolution down to μm scale [12]. For heavy ions even sub- μm level spatial resolution can be achieved [14]. Spectral information of deposited energy is provided for each particle with energy resolution for charged particles at the 4 % level [7].

4 Conclusions

The spectral and time sensitive imaging of ion microbeams has been examined with the Timepix detector. Quantum imaging sensitivity is provided by the detector high granularity and dark current free detection at the pixel level. Beam spot spatial and time patterns at the μm and μs levels can be inspected and independently monitored with a miniaturized detector operating in vacuum and at room temperature. The position of single particles is determined with sub-pixel spatial resolution down to the μm level. The resulting image size and image spatial bin are given by the detector spatial resolution and event rate (total fluence). A complete and precise characterization of the delivered microbeam is provided in terms of beam/radiation field composition, particle flux, deposited energy and beam spot homogeneity in terms of spatial and time distribution. Ion microbeams of varying configuration can be inspected. The method can be applied for ion beam lithography and online beam profile monitoring of delivered particle beams of low intensity (flux below 10^5 particles/cm²/s). At this particle flux no radiation damage or distortion of the detector spectral response is observed. For particle beams of higher energy, when the delivered particles have large range and cross the detector sensor thus producing elongated tracks, also the directional mapping of particles incident on the detector can be measured and

evaluated. For the Timepix detector used, with a 300 μm thick silicon sensor, this case occurs for protons of energy 8 MeV and light ions of energy above 10 MeV/u.

In addition to the inspection of beam size and spatial- and time- profile, the divergence of particle beams can be also examined and imaged together with information on the beam composition and deposited dose distributions. Future work includes processing and evaluation of additional data with Tandetron microbeams at other settings and beam spot ranges. Also, the use of the newly available Timepix3 ASIC chip, which provides two per-pixel signals, enables to register simultaneously both the deposited energy and time at the pixel level. Timepix3 will enable to resolve pile-up and spatially-overlapping events in the detector. Also, more particles can be registered thanks to the Timepix3 hit-pixel readout stream architecture which greatly reduces detector readout dead time.

Work by C.G. and C.O. was performed in frame of Contract No. 40001250020/18/NL/GLC/hh by the European Space Agency. Measurements at the Tandetron accelerator were carried out in frame of the CANAM infrastructure of the NPI CAS Rez, Research Infrastructure project No. LM2015056 of the Ministry of Education, Youth and Sports of the Czech Republic. We thank Jack Miller from the Lawrence Berkeley National Laboratory, USA, for English proof-reading and comments. We are grateful to the reviewers for remarks and valuable suggestions.

References

1. O. Romanenko et al., Rev. Sci. Inst. **90**, 013701 (2019)
2. R. Ortega, et. al., NIM-B **181**, 475-479 (2001)
3. J. Baglin, App. Surface Science **258**, 4103-4111 (2012)
4. X. Llopart, R. Ballabriga, M. Campbell, NIM-A **581**, 485-494 (2007)
5. C. Granja, J. Jakubek, S. Polansky, et al., NIM-A **908**, 60-71 (2018)
6. C. Granja, K. Kudela, J. Jakubek, et al., NIM-A **911**, 142-152 (2018)
7. C. Granja, C. Oancea, J. Jakubek, et. al., NIM-A **988**, 164901 (2021)
8. C. Granja, J. Jakubek, M. Martisikova, et. al., JINST **13**, C11003 (2018)
9. V. Patera, A. Sarti, IEEE TNS **40**, 133-146 (2020)
10. T.Y. Hsiao, H. Niu, T.Y. Chen, C.H. Chen, MethodsX **7**, 100773 (2020)
11. A. Natochii, F. Murtas, W. Scandale, J. Alozy, JINST **14** P03018 (2019)
12. J. Jakubek, A. Cejnarova, T. Holy, et. al., NIM-A **591**, 155-158 (2008)
13. V. Olsansky, C. Granja, C. Oancea, et. al., these proceedings (2022) *submitted*
14. C. Granja, J. Jakubek, S. Pospisil, et. al., NIM-A **574**, 472-478 (2007)